Journal of Organometallic Chemistry 693 (2008) 3643–3649

Contents lists available at ScienceDirect

Journal of Organometallic Chemistry

journal homepage: www.elsevier.com/locate/jorganchem

Tris(trimethylsilyl)silyl versus tris(trimethylsilyl)germyl: Radical reactivity and oxidation ability

Jacques Lalevée [a,*], Nicolas Blanchard [b], Bernadette Graff [a], Xavier Allonas [a], Jean Pierre Fouassier [a]

[a] Department of Photochemistry, UMR CNRS 7525, University of Haute Alsace, ENSCMu, 3 rue Alfred Werner, 68093 Mulhouse Cedex, France
[b] Department of Organic and Bioorganic Chemistry, UMR CNRS 7015, University of Haute Alsace, ENSCMu, 3 rue Alfred Werner, 68093 Mulhouse Cedex, France

ARTICLE INFO

Article history:
Received 22 July 2008
Received in revised form 28 August 2008
Accepted 29 August 2008
Available online 10 September 2008

Keywords:
Radical chemistry
Silyl radical
Germyl radical
Laser flash photolysis
Oxidation

ABSTRACT

A comparison of the tris(trimethylsilyl)silyl **I** and tris(trimethylsilyl)germyl **II** radical reactivity is provided. Their formation as well as their reactivity encountered in a large variety of chemical processes (addition to double bond, halogen abstraction, peroxyl radical formation...) is examined by laser flash photolysis, quantum mechanical calculations and electron spin resonance (ESR) experiments. The starting compound $(TMS)_3GeH$ is more reactive than $(TMS)_3SiH$ toward the *t*-butoxyl, the *t*-butylperoxyl and the phosphinoyl radicals. A similar behavior is noted for an aromatic ketone triplet state. **II** exhibits a lower absolute electronegativity: accordingly, the addition to electron rich alkenes is less efficient than for **I**. Radical **II** is also found less reactive for both the peroxylation ($\mathbf{II} + O_2 \rightarrow \mathbf{II}\text{-}O_2^{\cdot}$) and the halogen abstraction reactions. The rearrangement of $\mathbf{II}\text{-}O_2^{\cdot}$ is slower than for $\mathbf{I}\text{-}O_2^{\cdot}$; this is related to the respective exothermicity of the processes.

1. Introduction

Since its introduction as an efficient radical-based reducing agent more than twenty years ago, tris(trimethylsilyl)silane has found multiple applications in organic synthesis as well as in polymers and materials science [1–7]. Due to its low toxicity (compared to *n*-tributyltin hydride) and the very mild reaction conditions, tris(trimethylsilyl)silane has been a reagent of choice for the reduction reaction of organic halides, selenides, activated hydroxy- and carboxy groups even in aqueous media [1e]. The unique reactivity of tris(trimethylsilyl)silane has also been exploited in cascade reactions leading in a single step to complex molecular scaffolds. Recent elegant examples for nature products synthesis have been also reported [3]. In sharp contrast, tris(trimethylsilyl)germane has been much less exploited in organic synthesis even though its reactivity is slightly superior to *n*-tributyltin hydride [4]. Excellent yields were obtained in reduction reactions of secondary or tertiary halides, isonitriles, nitro or seleno moieties. Recently, tris(trimethylsilyl)germane was used in the radical-mediated germyldesulfonylation of vinylsulfones, thereby constituting a straightforward access to vinylgermanes, reactive partners in palladium-catalyzed cross-coupling reactions with aryl halides [4b–c].

We have recently found that both structures can be used as efficient co-initiators of free radical polymerization processes and efficient photosensitizing species in free radical promoted cationic photopolymerization. The intrinsic high reactivity of the generated radicals associated with the rearrangement of the peroxyls formed in aerated conditions (that regenerates the silyl or germyl radicals) [5–7] allow highly efficient initiation processes even under air.

The aim of the present paper corresponds to an investigation of the relative reactivity of tris(trimethylsilyl)silane $(TMS)_3Si–H$ and tris(trimethylsilyl)germane $(TMS)_3Ge–H$ (Scheme 1); the tris(trimethylsilyl)methane $(TMS)_3C–H$ is partly introduced for comparison. The formation of the silyl and germyl radicals will be investigated by laser flash photolysis and ESR spin trapping experiments ESR-ST. The rate constants of interaction with different additives (various monomers, lauraldehyde, diphenyliodonium hexafluorophosphate, CBr_4) will be determined to provide a coherent picture of the $Si^{\cdot}$ and $Ge^{\cdot}$ reactivity for a large range of processes. Finally, the behavior under air of these compounds will be investigated. Quantum mechanical calculations will help to understand the observed reactivity.

2. Experimental

The starting compounds (tris(trimethylsilyl)silane $(TMS)_3SiH$; tris(trimethylsilyl)germane $(TMS)_3GeH$; tris(trimethylsilyl)methane $(TMS)_3CH$) were obtained from Aldrich and used with the best purity available. In the case of liquid monomers – vinyl ethyl ether

* Corresponding author. Tel.: +33 3 89 33 68 37; fax: +33 3 89 33 68 95.
E-mail address: j.lalevee@uha.fr (J. Lalevée).

0022-328X/$ - see front matter © 2008 Elsevier B.V. All rights reserved.
doi:10.1016/j.jorganchem.2008.08.039

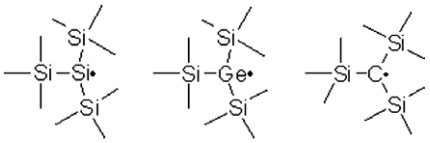

I II III

Scheme 1.

VE, vinyl acetate VA, methyl acrylate MA, acrylonitrile AN – (purchased from Aldrich), the stabilizer (4-methoxyphenol) was removed by column purification (Aldrich AL-154). Lauraldehyde (LA), diphenyliodonium hexafluorophosphate (Φ_2I^+), CBr_4, 4-methoxyphenol (4-MeOP) and vitamin E (Vit E) were also obtained from Aldrich.

2.1. Laser flash photolysis

The silyl or germyl radical reactivity was studied by nanosecond laser flash photolysis at RT (using the equipment described in [8]; resolution time: 10 ns). The solvent used is di-*tert*-butylperoxide/benzene (50%/50%) and acetonitrile for the experiments with *t*Bu–O· and P·, respectively (see text below). The interaction of $(TMS)_3GeH$ and $(TMS)_3SiH$ with a ketone triplet state (benzophenone BP) was studied in benzene; the ketyl radical quantum yield Φ_K. In the case of benzophenone was determined by a classical procedure [8].

2.2. Kinetic ESR (KSER)

The ESR experiments were carried out using a X-band spectrometer (MS 200 from Magnettech-Berlin; Germany) at room temperature. The radicals were generated through photolysis in an air saturated inert solvent (*tert*-butylbenzene). During the photolysis, the spectrometer was set at the magnetic field corresponding to the maximum peak height of the first derivative of the observed radical and the field sweep was switched off. Decays in the signal were monitored when the light was interrupted. The kinetic ESR (KESR) procedures have been described in detail in [9a–e]. The interaction rate constants of *t*Bu–OO· with $(TMS)_3GeH$; $(TMS)_3SiH$ and $(TMS)_3CH$ were determined from the lifetime of *t*Bu–OO· at different quencher concentrations through a classical Stern–Volmer plot. The starting radical formed from the photolysis of 2,2,4,4-tetramethylpent-3-one in an oxygenated medium is observed at $g = 2.015$ [9a–b].

2.3. ESR spin trapping experiments

This ESR technique (ESR-ST) is now recognized as particularly powerful for the identification of the radical centers [9f–g]. The radicals generated under light exposure of a Xe–Hg lamp (Hamamatsu, L8252, 150 W; $\lambda > 310$ nm) were trapped by phenyl-*N*-*t*-butylnitrone (PBN). *Tert*-butylbenzene was used as a solvent. ESR spectra simulations were carried out with the WINSIM software [10].

2.4. Redox potentials

The redox potentials were measured in acetonitrile by cyclic voltammetry with tetrabutyl-ammonium hexafluorophosphate 0.1 M as supporting electrolyte (Voltalab 06-Radiometer; the working electrode was a platinium disk and the reference a saturated calomel electrode-SCE). Ferrocene was used as a standard and the potentials determined from the half peak potential were referred to the reversible formal potential of this compound (+0.44 V/SCE).

2.5. Hydroperoxides formation under air

The formation of the hydroperoxides in benzophenone/$(TMS)_3SiH$ or benzophenone/$(TMS)_3GeH$ in acetonitrile under light irradiation (Hg–Xe lamp, 120 s, $I \sim 20$ mW/cm^2) and under air was studied through a classical iodometric determination [11]. After irradiation, the concentration in hydroperoxides was determined by addition of NaI through the following redox reaction sequence:

$$ROOH + I^- \rightarrow RO^{\cdot} + OH^- + I_2$$
$$I_2 + I^- \rightarrow I_3^-$$

The absorbance of the solutions was then measured with a UV–Vis spectrometer (Beckman 640) at 358 nm (typical of I_3^-). In acetonitrile, a molar extinction coefficient of 29 400 M^{-1} cm^{-1} was first determined [11].

2.6. DFT calculations

All the calculations were performed using the hybrid functional B3LYP from GAUSSIAN 03 suite of program [12]. Reactants and products were fully optimized at the B3LYP/6-31+G* level (and frequency checked). For the calculation of the transition states (TS) for the peroxyl radical rearrangement, the QST2 procedure, described in detail in [12], was used. The peroxyl radicals absorption spectra were calculated at TD(Nstates = 10)MPW1PW91/6-31+G* level.

3. Results and discussions

3.1. Generation of the silyl and germyl radicals

The generation of the silyl or germyl radicals can arise according to different ways [13–16]. All these approaches are based on a hydrogen abstraction reaction by the *tert*-butoxyl radical *t*Bu–O· (reaction 1 in Scheme 2) [13–14], the phosphinoyl radical P· (reaction 2 in Scheme 2) or the benzophenone ^{3}BP triplet state (reaction 3 in Scheme 2). A general review of the hydrogen donor abilities of the group 14 hydrides has been presented in [15a]. The interaction of *t*Bu–O· with $(TMS)_3SiH$ and $(TMS)_3GeH$ as hydrogen donors D–H yields **I** or **II**: their absorption (known as usually weak for $\lambda > 300$ nm) [15–16] can however be followed at 330 nm (Fig. 1). The rise time of this absorption allows the evaluation of the interaction rate constants (Table 1). For reactions 2 and 3, the interaction rate constants k_H are extracted from the decay times of P· or ^{3}BP observed at 450 and 525 nm in acetonitrile, respectively (Table 1 and Fig. 1). The phosphinoyl radical is easily generated by the di-

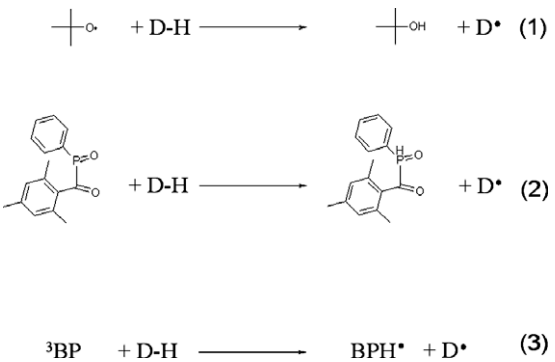

Scheme 2.

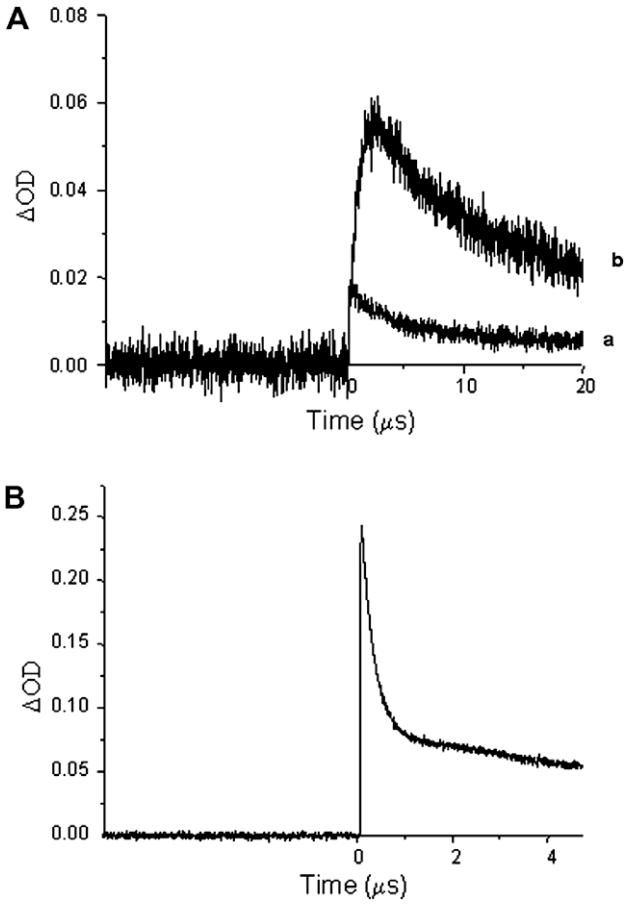

Fig. 1. LFP experiments. (A) Decay traces monitored at 330 nm as a function of [MA]; (a) for the germyl radical **II** ([MA] = 0 M) and (b) for the adduct **II**-MA· ([MA] = 0.062 M). (B) Decay trace of ^{3}BP at [$(TMS)_3$Ge-H] = 0.002 M.

rect cleavage of phenyl-bis(2,4,6-trimethylbenzoyl) phosphine oxide at 355 nm [17]. For reaction 3, the ketyl radical quantum yields Φ_K (also equal to the quantum yields in **I** or **II**) are also given in Table 1. The interaction rate constants of *t*-butylperoxyl *t*BuOO· with $(TMS)_3$SiH and $(TMS)_3$GeH were obtained from KESR experiments since alkylperoxyls absorb in a spectral window hardly accessible by a LFP setup [13c].

Concerning the reaction with *t*-Bu–O·, *t*-BuOO·, P· and ^{3}BP, $(TMS)_3$GeH is found more reactive than $(TMS)_3$SiH with relative rate constant ratios ~5, 3, 50, 10, respectively. This can be ascribed to the bond dissociation energy BDE (Ge–H) which is calculated lower than the BDE (Si–H) thereby rendering the corresponding abstraction process more exothermic (Table 1). A similar behavior was noted for the reactivity of primary alkyl radicals with $(TMS)_3$SiH and $(TMS)_3$GeH [15e]. The calculated BDE are in reasonable agreement with the experimental data (Table 1) [18]. Interestingly, P· is found more selective than *t*-Bu–O·. This is likely due to a higher reaction exothermicity for *t*-Bu–O· associated with the fact that BDE(O–H) > BDE (P(O)–H) [18]. A very high reactivity of alkylperoxyls with the Si–H and Ge–H functions is noted (Fig. 2 in Supplementary material). The values found are different to those obtained in [22] with a different approach (inhibited hydrocarbon oxidation methodologies): 66 and 4000 M^{-1} s^{-1} for $(TMS)_3$SiH and $(TMS)_3$GeH, respectively. This method is also well known for the evaluation of the ROO· interaction rate constants. This method is based on a kinetic scheme. The reasons for the deviation between KESR and the inhibited oxidation procedure are not known here. Further works are probably necessary to understand this behavior. The rate constants can also be advantageously compared to those found for alkanes ($k < 1$ M^{-1} s^{-1}) [19]: this demonstrates the intrinsic reactivity of both structures for the auto-oxidation processes (see Section 3.4).

In the case of ^{3}BP, the radical quantum yields are very high (>0.8). The rate constant found with $(TMS)_3$GeH (in the 10^9 M^{-1} s^{-1} range) appears, however, as rather high for a pure hydrogen abstraction reaction. This can be due to the lower oxidation potential of this specie (E_{ox} = 1.44 V, Table 1) leading to an electron–proton transfer sequence for the overall hydrogen abstraction process or at least to a high charge transfer character for the hydrogen transfer. Indeed, the free energy change for a possible electron transfer process (ΔG_{et}) can be evaluated from the classical Rehm–Weller equation (Eq. (1), where E_{ox}, E_{red}, E_T and C are the oxidation potential of the donor, the reduction potential of the acceptor, the triplet state energy and the coulombic term for the formed initial ion pair, respectively [20]; C was neglected here)

$$\Delta G_{et} = E_{OX} - E_{red} - E_T + C \quad (1)$$

Using for BP a reduction potential and a triplet energy level of 1.79 V and 2.98 eV, respectively [20b], the ΔG_{et} values of +0.25 and +0.51 eV are calculated for $(TMS)_3$GeH and $(TMS)_3$SiH, respectively. From these results, it can be noted that, despite an endergonic process, a quite low ΔG_{et} value is associated with the germane derivative rendering feasible the electron transfer process, in agreement with the high rate constant.

In comparison, the behavior of $(TMS)_3$C–H was examined. The hydrogen abstraction rate constants with *t*BuO·, *t*BuOO·, P· and ^{3}BP are much lower than for Si–H and Ge–H (Table 1). This can be ascribed both to a high BDE(C–H) (414.7 kJ/mol) and/or a higher E_{ox} rendering the hydrogen transfer or the electron proton transfer sequence not exothermic enough. As the formation of this radical cannot be observed, no other data are available.

The **I** and **II** radicals were also characterized by the ESR-ST technique for reactions 1–3 (Scheme 2). For these processes, the adducts were trapped with PBN, the corresponding hyperfine splitting constants a_H and a_N are gathered in Table 1. It is particularly worthnoting that a_H is found much higher for **II** i.e. 9.85 versus 5.7 G for **II** and **I**, respectively.

3.2. Structures of *I* and *II*

I and **II** have been characterized by DFT calculations. These radicals exhibit a pyramidal structure as evidenced by the dihedral

Table 1
Rate constants and parameters characterizing the radical formation in benzene at RT

	BDE[a] (kJ/mol)	k_H (*t*-Bu–O·) (10^7 M^{-1} s^{-1})	k_H (*t*Bu–OO·) (M^{-1} s^{-1})	k_H (P·) (10^7 M^{-1} s^{-1})	k_H (^{3}BP) (10^7 M^{-1} s^{-1})	Φ_K	E_{ox} (V/SCE)	HFS (G)
I	334.0 (350.3)	8.5	590	0.87	10.2	0.95	1.7	a_N = 15.2; a_H = 5.7
II	316.8 (305.9)	45.0	1790	44	105	0.81	1.44	a_N = 14.85; a_H = 9.85
III	414.7	<0.03	<1	<0.1	<0.05	n.d.	>2	[b]

n.d. not determined (almost no quenching is observed).
[a] Determined at UB3LYP/6-31+G* level; in brackets the experimental data from [18].
[b] Not trapped.

angle (α) between the plan characterized by the two silicon atoms and the radical center (Si or Ge) and the third silicon atom as depicted in Fig. 2. For a planar radical structure, α must be 180°. For **I** and **II**, α is 156 and 150°, respectively. The bent out of the plane structure of the germyl radical is more pronounced. These results can be compared to the value found (171°) for $(TMS)_3C^{\cdot}$. This general property of the silyl and germyl radicals was already known: the main difference between C·, Si· and Ge· arises from the fact that C· can only use 2s and 2p atomic orbitals to accommodate the valence electrons whereas Si· and Ge· can use s, p and d orbitals. The shapes of the silyl or germyl radicals are normally considered to be strongly bent out of the plane (σ type structure).[1a] Interestingly, this behavior is enhanced for **II**. This can be ascribed to the 3d orbitals which are already occupied and the possible extension of the 4d orbital. For $(TMS)_3C^{\cdot}$, an almost planar structure is obtained. The deviation from planarity for C· can be due to the steric hindrance associated with the TMS groups. The calculated spin density for the radical centers is 0.85; 0.98 and 1.1 for **I**, **II** and **III**, respectively. This demonstrates that the maximal delocalization is observed for **I**.

3.3. Reactivity of *I* and *II* toward different additives

The radicals were generated from the hydrogen abstraction with *t*-BuO·. The reactivity of **I** and **II** was investigated by LFP for different processes: (i) the addition to different double bonds (C=C) or (C=O) (Scheme 3) (ii) the addition to oxygen leading to a peroxyl radical formation, (iii) the halogen abstraction from CBr_4 and (iv) the oxidation of these radicals by Φ_2I^+ ($\mathbf{I} + \Phi_2I^+ \rightarrow \mathbf{I}^+ + \Phi^{\cdot} + \Phi$-I). The comparison of the **I**/**II** reactivity for these different processes can be useful to get a coherent picture of the respective behavior of the silyl or germyl radicals.

The rate constants *k* for the processes (i) and (ii) were determined from the rising time of the adducts corresponding to these reactions as the adducts absorb much more strongly than the starting radical (Fig. 1) [14a]. For the processes (iii) and (iv), they were determined from the decay time of **I** or **II** directly observed at 330 nm. The rate constants are gathered in Table 2.

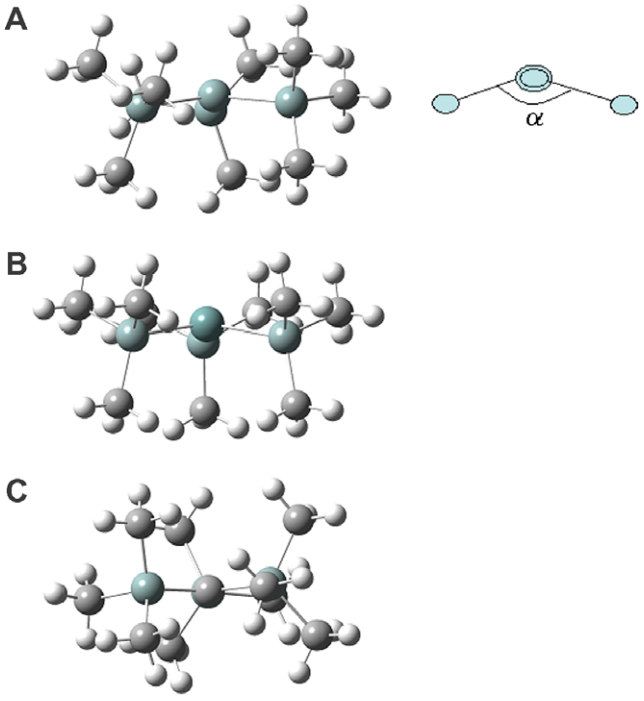

Fig. 2. Structures of the radicals: (A) **I**, (B) **II**, (C) $(TMS)_3C^{\cdot}$ at UB3LYP/6-31+G* level. The definition used for the dihedral angle α is also given.

Scheme 3.

In the addition of **I** and **II** to alkenes, a high reactivity is noted (Table 2). For acrylonitrile AN and methyl acrylate MA (alkenes bearing withdrawing substituents) a very similar reactivity is found for **I** and **II**. For vinyl acetate VA and vinyl ether VE (electron rich alkenes), **I** is more reactive than **II**. This can evidence the higher electrophilic character of **I**. This is in agreement with the higher absolute electronegativity calculated for **I** (4.06 eV and 3.70 eV at UB3LYP/6-31+G* level for **I** and **II**, respectively) [13–14].

As observed for the addition of other silyl radicals to a ketone double bond [1a], it can be assumed that the addition to the C=O bond of lauryl aldehyde LA occurs at the oxygen atom with the formation of a carbon centered radical. A low reactivity is noted for **I** and **II** ($k < 6 \times 10^6\ M^{-1}\ s^{-1}$); it can be compared to that found for $Ph_3Si^{\cdot}$ and $Ph_3Ge^{\cdot}$: 6.2×10^7 and $9.5 \times 10^6\ M^{-1}\ s^{-1}$, respectively. The lower calculated addition exothermicity for **I** and **II** (−73.1 and −138.1 kJ/mol for **I** and $Ph_3Si^{\cdot}$, respectively) is presumably responsible of this behavior. For **I**, the addition to the oxygen atom is found more exothermic than that for a carbon atom (by 53.4 kJ/mol) in agreement with the expected selectivity.

In the halogen abstraction from CBr_4, the rate constant is higher for **I** ($34 \times 10^7\ M^{-1}\ s^{-1}$). This can be in line with the higher BDE (Si–Br) compared to BDE (Ge–Br) rendering the abstraction process more exothermic [18].

In the radical oxidation with Φ_2I^+, a quite high rate constant ($0.26 \times 10^7\ M^{-1}\ s^{-1}$) is obtained with **I** in agreement with the low ionization potential IP usually assumed for silyl radicals [1a]. For **II**, an upper value of $2 \times 10^7\ M^{-1}\ s^{-1}$ can only be given: the degradation of the solution under light irradiation prevents a more refined analysis. The IP of **II** is calculated lower than for **I** (6.0 versus 6.36 eV for **I**): this likely demonstrates that germyl radicals can also be oxidized by an aryliodonium salt. This result is in agreement with the photosensitization of a cationic polymerization recently observed when using these radicals [7].

3.4. Oxidation process of $(TMS)_3SiH$ and $(TMS)_3GeH$

3.4.1. Laser flash photolysis investigation

Under air, the *t*BuO·/$(TMS)_3SiH$ and *t*BuO·/$(TMS)_3GeH$ interactions lead to new transients with a maximum absorption at 420 and 390 nm, respectively (Figs. 3 and 4). From the measurement of the radical rising time at various $[O_2]$, the interaction rate con-

Table 2
Rate constants k for the reaction of the radicals I and II with various additives in di-*tert*-butylperoxide

	I $10^7\ k\ (M^{-1}\ s^{-1})$	**II** $10^7\ k\ (M^{-1}\ s^{-1})$
AN	5.1	4.5
MA	2.2	3.4
VA	0.12	<0.05
VE	0.02	<0.05
LA	<0.6	<0.6
O_2	200	39
CBr_4	34	8
Φ_2I^+	0.26	<2

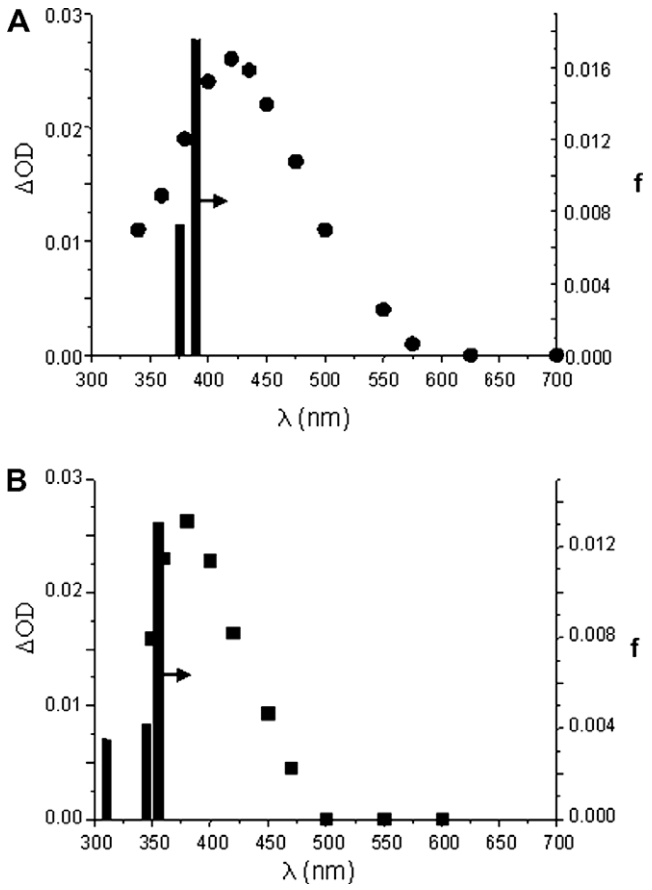

Fig. 3. Transient peroxyl radical spectra associated with **I** (A) and **II** (B) in di-*tert*-butylperoxide (oxygen saturated solution, $[(TMS)_3SiH] = 0.05$ M; $[(TMS)_3GeH] = 0.05$ M). The calculated peroxyl radical spectra are given (black bar): λ_{max} and oscillator strength (f) at TD-DFT/MPW1PW91/6-31+G* level.

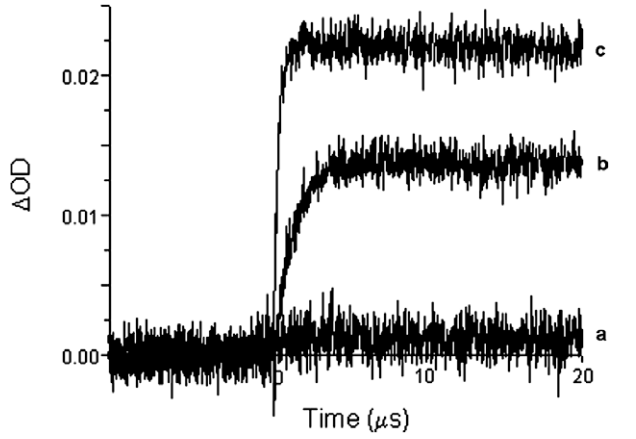

Fig. 4. Building up of the transient **II**-$O_2^{\cdot}$ absorption in di-*tert*-butylperoxide (a) under argon, (b) in aerated solution ($[O_2] = 0.0019$ M) and (c) in saturated oxygen solution ($[O_2] = 0.0091$ M).

stants for **I**/O_2 and **II**/O_2 are determined as 2×10^9 and 3.9×10^8 M^{-1} s^{-1}. The observed new transients are ascribed to the corresponding peroxyl radicals as the calculated and experimental absorption spectra are in good agreement (Fig. 3). It is worthnoting that the absorption of these peroxyls are red shifted compared to the classical absorption of alkylperoxyl radicals ($\lambda < 270$ nm) [13c,13d,21]: this is ascribed to a partial charge transfer transition.

Interestingly, the lifetime of **I**-$O_2^{\cdot}$ is found short (about 2.5 μs) compared to **II**-$O_2^{\cdot}$ (>5 ms). For **I**-$O_2^{\cdot}$, it has been already suspected that a fast rearrangement (competitive to the possible formation of a hydroperoxide) occurs with the migration of a trimethylsilyl (TMS) substituent (Scheme 4 as proposed in [22] albeit no direct kinetic information is available) leading to a silyloxyl radical ***A*** and then a silyl radical ***B***. This Scheme was originally proposed in agreement with $^{16}O_2$, $^{18}O_2$ labeling experiments [22]. This rearrangement appears less favorable for the germyl structure as **II**-$O_2^{\cdot}$ has a much higher lifetime (Fig. 3 in Supplementary material).

To shed some light on this behavior, the associated reorganization enthalpies have been calculated at UB3LYP/6-31+G* level. Interestingly, it is clearly found that the TMS group migration process is more exothermic for **I**-$O_2^{\cdot}$ (−462 kJ/mol) compared to **II**-$O_2^{\cdot}$ (−340 kJ/mol) in agreement with the respective peroxyl stability. The basic difference is the lower BDE (Ge–O) compared to BDE (Si–O) calculated as 397.6 and 446.1 kJ/mol for $CH_3Ge–OCH_3$ and $CH_3Si–OCH_3$ (at UB3LYP/6-31+G* level). The transition states corresponding to the TMS group migration (reaction from the metal peroxyl M–O–O· to the structure noted ***A*** in Scheme 4) were calculated; the TS structures are given in the Supplementary material. The barrier calculated at UB3LYP/6-31+G* is found lower for **I**-$O_2^{\cdot}$ (50.1 kJ/mol) than for **II**-$O_2^{\cdot}$ (122.2 kJ/mol). This is in full agreement with the shorter lifetime of **I**-$O_2^{\cdot}$.

The direct observation of the peroxyl radicals can be valuable for a direct access to their chemical reactivity. Due to its short lifetime, **I**-$O_2^{\cdot}$ is not a convenient probe for the evaluation of the low rate constants (upper values in the 10^7 M^{-1} s^{-1} range can only be obtained). The interaction with different additives (4-methoxy phenol, vitamin E and Φ_2I^+) has been investigated using **II**-$O_2^{\cdot}$ which is characterized by a much longer lifetime (Table 3). The reaction with 4-MeOP or vitamin E is quite efficient (about 10 times higher than that noted for alkyl peroxyls) [13c,21]. The same behavior is found for Φ_2I^+. This evidences the high reactivity of this metal peroxyl radical.

3.4.2. ESR spectra under air

The ESR results obtained under air confirm the information gained through LFP. For **I**, a spectrum characterized by $g \approx 2.0045$ is recorded (Fig. 5) and is safely assigned to the final silyl radical (specie ***B*** in Scheme 4) the *g* factor being in the typical range known for Si· radicals [1a]. Moreover, this *g* value is too low for a peroxyl radical (usually in the 2.011–2.015 range for C–OO· and 2.020–2.025 for Si–OO·) [23]. For **II**, a specie characterized by

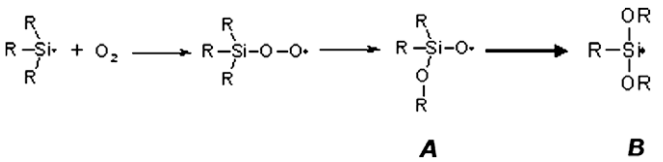

Scheme 4.

Table 3
Rate constants k for the reaction of the peroxyl radicals (derived from **II**) with various additives in di-*tert*-butylperoxide

	II-$O_2^{\cdot}$ 10^6 k (M^{-1} s^{-1})
Rearrangement	<0.001[a] (0.00001[b])
$k_{(4MeOP)}$	0.11
$k_{(Vit\ E)}$	5.5
$k_{(\Phi 2I+)}$	1.0

[a] In s^{-1}.
[b] KESR data.

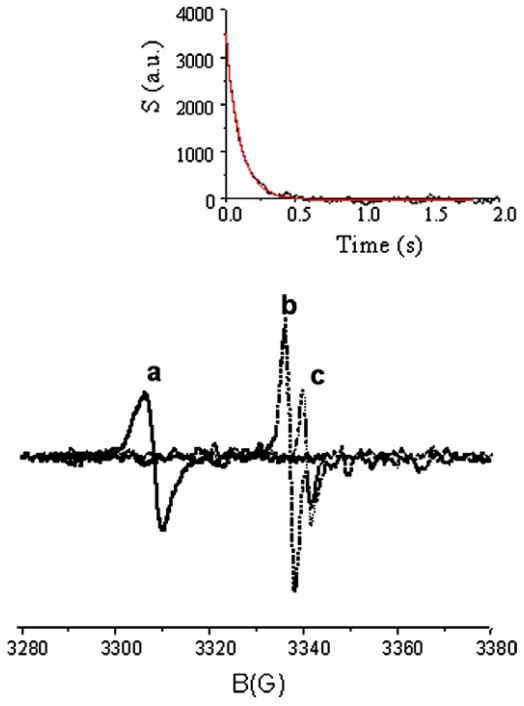

Fig. 5. ESR spectra recorded under air in di-*tert*-butylperoxide for (a) $(TMS)_3GeH$ (0.02 M); (b) $(TMS)_3SiH$ (0.02 M); (c) $(TMS)_3CH$ (0.040 M). The *g* calibration was carried out with tetramethylpiperidine *N*-Oxyl (TEMPO) as a reference. Insert: decay of **II**-$O_2^{\cdot}$ at 3306.5 G observed by kinetic ESR (KESR).

$g = 2.021$ is observed: this high *g* value is typical of a germylperoxyl structure (i.e. for the trimethylgermylperoxyl, a broad singlet ESR spectrum centered at $g = 2.0245$ was already observed in [23]). The decay of **II**-$O_2^{\cdot}$ observed by KESR (Fig. 5) can be fitted by an exponential decay (radical lifetime: 99 ms). This leads to a reorganization rate constant of $\sim 10\ s^{-1}$ (Scheme 4). This is in agreement with the LFP results for which a much shorter lifetime for **I**-$O_2^{\cdot}$ was observed. Due to the time resolution of our equipment (actually about 1 ms), the decay of **I**-$O_2^{\cdot}$ cannot be followed here.

For the *t*BuO$^{\cdot}$/$(TMS)_3CH$ system under air, the specie detected is typical of a carbon centered radical (Fig. 5) [23]. This result evidences the formation of $(TMS)_3C^{\cdot}$. As the formation of peroxyls is not observed, a low reactivity of $(TMS)_3C^{\cdot}$ toward O_2 is expected. This is in contrast with the almost diffusion controlled reactions (~ 3–$4 \times 10^9\ M^{-1}\ s^{-1}$) often observed for the addition of carbon centered radicals to O_2. This behavior is probably ascribed to the steric hindrance associated with a C$^{\cdot}$ radical bearing TMS bulky substituents.

3.4.3. Hydroperoxide formation

The formation of hydroperoxides in BP/$(TMS)_3SiH$, BP/$(TMS)_3GeH$, BP/Ph_3SiH and BP/Ph_3GeH in acetonitrile upon light irradiation under air was investigated. Contrary to BP/Ph_3SiH and BP/Ph_3GeH, the I_3^- anion is not detected in BP/$(TMS)_3SiH$ and BP/$(TMS)_3GeH$: the hydroperoxide formation (**I**-$O_2^{\cdot}$ + **I**-H → **I**$^{\cdot}$ + **I**-O_2H) is low (<1% to the quantity observed for Ph_3SiH or Ph_3GeH) and can be neglected. This is a strong evidence for the competitive rearrangement of **I**-$O_2^{\cdot}$ and **II**-$O_2^{\cdot}$. This also demonstrates that the reorganization process for **II**-$O_2^{\cdot}$ is the major pathway governing the decay of this specie despite a quite low rate constant. In the case of Ph_3SiH and Ph_3GeH, a phenyl migration in the corresponding peroxyls is probably not favourable and hydroperoxides are observed. This is in agreement with the higher lifetime for $Ph_3GeOO^{\cdot}$ observed here by KESR at $g = 2.028$ (>2 s and decaying by a second order kinetics supporting the usual recombination process).

4. Conclusion

In the present paper, the reactivity of two selected silane and germane compounds was examined and compared through the determination of the reaction rate constants of the processes. Among the gathered new information, the oxidation behavior was specifically investigated: it underlines the rearrangement of the peroxyls which is concomitant with a low hydroperoxide formation. All this new approach based on a direct access to the radicals reactivity (as the Si and Ge peroxyl radicals were for the first time observed by LFP) should be useful for a better understanding of the associated behavior under air. The use of silyl or germyl radicals as polymerization initiating species in aerated media will be discussed in forthcoming papers.

Acknowledgments

The authors thank the CINES (Centre Informatique National de l'Enseignement Supérieur) and IDRIS (Institut du Développement et des Ressources en Informatique Scientifique-CNRS) for the generous allocation of time on the IBM SPsupercomputer.

Appendix A. Supplementary material

(i) Use of $(TMS)_3SiH$ as reported by Nicolaou in his synthetic efforts towards azadirachtin [3]. (ii) Transition states corresponding to the TMS group migration (reaction from the metal peroxyl M–O–O$^{\cdot}$ to the structure noted ***A*** in Scheme 4). (iii) KESR experiments for the *t*-BuO–O$^{\cdot}$/$(TMS)_3SiH$ interaction. (iv) Peroxyl radical decays in LFP experiments: **I**-OO$^{\cdot}$ and **II**-OO$^{\cdot}$. Supplementary data associated with this article can be found, in the online version, at doi:10.1016/j.jorganchem.2008.08.039.

References

[1] (a) C. Chatgilialoglu, in: Organosilanes in Radical Chemistry, Wiley, Chichester, 2004;
(b) J. Fossey, D. Lefort, J. Sorba, in: Free Radicals in Organic Chemistry, Wiley&Sons, New York, 1995;
(c) S.Z. Zard, in: Radical reactions in Organic Synthesis, Oxford University Press, Oxford, UK, 2003;
(d) C. Chatgilialoglu, in: P. Renaud, M.P. Sibi (Eds.), Radicals in Organic Synthesis, vol.1, Wiley-VCH, Weinheim, Germany, 2001, pp. 28–49;
(e) A. Postigo, S. Kopsov, C. Ferreri, C. Chatgilialoglu, Org. Lett. 9 (2007) 5159.
[2] (a) C. Chatgilialoglu, Chem. Eur. J. 14 (2008) 2310;
(b) C. Chatgilialoglu, Acc. Chem. Res. 25 (1992) 188;
(c) C. Chatgilialoglu, A. Guerrini, M. Lucarini, J. Org. Chem. 57 (1992) 3405;
(d) M. Ballestri, C. Chatgilialoglu, K.B. Clark, D. Griller, B. Giese, B. Kopping, J. Org. Chem. 56 (1991) 678.
[3] K.C. Nicolaou, P.K. Sasmal, T.V. Koftis, A. Converso, E. Loizidou, F. Kaiser, A.J. Roecker, C.C. Dellios, X.-W. Sun, G. Petrovic, Angew. Chem., Int. Ed. 44 (2005) 3447.
[4] (a) C. Chatgilialoglu, M. Ballestri, Organometallics 14 (11) (1995) 5017;
(b) S.F. Wnuk, P.I. Garcia Jr., Z. Wang, Org. Lett. 6 (2004) 2047;
(c) Z. Wang, S.F. Wnuk, J. Org. Chem. 70 (2005) 3281.
[5] J. Lalevée, M. El-Roz, F. Morlet-Savary, B. Graff, X. Allonas, J.P. Fouassier, Macromolecules 40 (2007) 8527.
[6] J. Lalevée, A. Dirani, M. El-Roz, X. Allonas, J.P. Fouassier, Macromolecules 41 (2008) 2003.
[7] J. Lalevée, A. Dirani, M. El-Roz, X. Allonas, J.P. Fouassier, J. Polym. Sci. Part A: Polym. Chem. 46 (2008) 2008.
[8] J. Lalevée, X. Allonas, J.P. Fouassier, J. Am. Chem. Soc. 124 (2002) 9613.
[9] (a) E. Furimsky, J.A. Howard, J. Am. Chem. Soc. 95 (1973) 369;
(b) B.W. Burton, T. Doba, E.J. Gabe, L. Hughes, F.L. Lee, L. Prasad, K.U. Ingold, J. Am. Chem. Soc. 107 (1985) 7053;
(c) S. Fukuzumi, K. Shimoosako, T. Suenobu, Y. Watanabe, J. Am. Chem. Soc. 125 (2003) 9074;
(d) J.A. Howard, Landolt Bornstein Numerical Data and Functional Relationships in Science and Technology, Group II, vol. 18, sub vol. D2, Springer-Verlag, Berlin, 1997;
(e) D. Griller, J.A. howard, P.R. Marriott, J.C. Scaiano, J. Am. Chem. Soc. 103 (1981) 619;
(f) P. Tordo, in: N.M. Atherton, M.J. Davies, B.C. Gilbert (Eds.), Electron Spin Resonance, vol. 16, The Royal Society of Chemistry, Cambridge, 1998;
(g) Y. Kotake, K. Kuwata, Bull. Chem. Soc. Jpn. 54 (1981) 394.

[10] D.R. Duling, J. Magn. Reson. Ser. B 104 (1994) 105.
[11] D.S. Breslow, D.A. Simpson, B.D. Kramer, R.J. Schwarz, N.R. Newburg, Ind. Eng. Chem. Res. 26 (1987) 2144.
[12] (a) GAUSSIAN 03, Revision B-2, M.J. Frisch, G.W. Trucks, H.B. Schlegel, G.E. Scuseria, M.A. Robb, J.R. Cheeseman, V.G. Zakrzewski, J.A. Montgomery Jr., R.E. Stratmann, J.C. Burant, S. Dapprich, J.M. Millam, A.D. Daniels, K.N. Kudin, M.C. Strain, O. Farkas, J. Tomasi, V. Barone, M. Cossi, R. Cammi, B. Mennucci, C. Pomelli, C. Adamo, S. Clifford, J. Ochterski, G.A. Petersson, P.Y. Ayala, Q. Cui, K. Morokuma, P. Salvador, J.J. Dannenberg, D.K. Malick, A.D. Rabuck, K. Raghavachari, J.B. Foresman, J. Cioslowski, J.V. Ortiz, A.G. Baboul, B.B. Stefanov, G. Liu, A. Liashenko, P. Piskorz, I. Komaromi, R. Gomperts, R.L. Martin, D.J. Fox, T. Keith, M.A. Al-Laham, C.Y. Peng, A. Nanayakkara, M. Challacombe, P.M.W. Gill, B. Johnson, W. Chen, M.W. Wong, J.L. Andres, C. Gonzalez, M. Head-Gordon, E.S. Replogle, J.A. Pople, GAUSSIAN, Inc., Pittsburgh PA, 2003;
(b) J.B. Foresman, A. Frisch, in: Exploring Chemistry with Electronic Structure Methods, 2nd ed., GAUSSIAN. Inc., 1996.
[13] (a) J. Lalevée, X. Allonas, B. Graff, J.P. Fouassier, J. Phys. Chem. A 111 (2007) 6991;
(b) J. Lalevée, X. Allonas, J.P. Fouassier, Chem. Phys. Lett. 415 (2005) 202;
(c) J. Lalevée, X. Allonas, J.P. Fouassier, Chem. Phys. Lett. 445 (2007) 62;
(d) J. Lalevée, X. Allonas, J.P. Fouassier, K.U. Ingold, J. Org. chem. 73 (2008) 6489.
[14] (a) J. Lalevée, X. Allonas, J.P. Fouassier, J. Org. Chem. 72 (2007) 6434;
(b) J. Lalevée, X. Allonas, F. Morlet-Savary, J.P. Fouassier, J. Phys. Chem. A 110 (2006) 11605.
[15] (a) C. Chatgilialoglu, M. Newcomb, Adv. Organomet. Chem. 44 (1999) 67;
(b) C. Chatgilialoglu, K.U. Ingold, J.C. Scaiano, J. Am. Chem. Soc. 105 (1983) 3292;
(c) C. Chatgilialoglu, K.U. Ingold, J.C. Scaiano, J. Am. Chem. Soc. 104 (1982) 5119;
(d) C. Chatgilialoglu, S. Rossini, Bull. Soc. Chim. Fr. 2 (1988) 298;
(e) C. Chatgilialoglu, M. Ballestri, J. Escudie, I. Pailhous, Organometallics 18 (1999) 2395.
[16] (a) C. Chatgilialoglu, M. Guerra, A. Guerrini, G. Seconi, K.B. Clark, D. Griller, J. Kanabus-Kaminska, J.A. Martinho-Simoes, J. Org. Chem. 57 (1992) 2427;
(b) C. Chatgilialoglu, K.U. Ingold, J. Lusztyk, A.S. Nazran, J.C. Scaiano, Organometallics 2 (1983) 1332.
[17] K. Dietliker, A Compilation of Photoinitiators Commercially Available for UV Today, Sita Technology Ltd., Edinburgh, London, 2002.
[18] (a) Y.R. Luo, Handbook of Bond Dissociation Energy in Organic Compounds, CRC Press, 2003;
(b) R. Beccera, R. Walsh, in: Z. Rappoport, Y. Apeloig (Eds.), The Chemistry of Organic Silicon Compounds, vol. 2, John Wiley & Sons, 1994 (Chapter 4);
(c) T.I. Drozdova, E.T. Denisov, Kinet. Catal. 43 (2002) 14.
[19] J.A. Howard, J.C. Scaiano, in: H. Fischer (Ed.), Landolt–Bornstein new series, group II, vol. 13, Radical Reaction Rates in Liquids, Part D, Springer-Verlag, Berlin, 1984, pp. 251–253.
[20] (a) D. Rehm, A. Weller, Israel J. Chem. 8 (1970) 259;
(b) S.L. Murov, I. Carmichael, G.L. Hug, Handbook of Photochemistry, Ed. Marcel Dekker Inc., New York, 1993.
[21] K.U. Ingold, Acc. Chem. Res. 2 (1969) 1.
[22] (a) A.B. Zaborovskiy, D.S. Lutsyk, R.E. Prystansky, V.I. Kopylets, V.I. Timokhin, C. Chatgilialoglu, J. Organomet. Chem. 689 (2004) 2912;
(b) C. Chatgilialoglu, A. Guarini, A. Guerrini, C.G. Seconi, J. Org. Chem. 57 (1992) 2207;
(c) C. Chatgilialoglu, A. Guerrini, M. Lucarini, G.F. Pedulli, P. Carrozza, G. Da Roit, V. Borzatta, V. Lucchini, Organometallics 17 (1998) 2169.
[23] (a) J.A. Howard, J.C. Tait, S.B. Tong, Can. J. Chem. 57 (1979) 2761;
(b) J.A. Howard, J.C. Tait, Can. J. Chem. 54 (1976) 2669;
(c) J.A. Howard, J.C. Tait, Can. J. Chem. 56 (1978) 2163.